EUROPEAN ORGANIZATION FOR NUCLEAR RESEARCH

CERN PPE/93-42
4 March 1993

Measurement of the $\bar{B}^0$ and B^- Meson Lifetimes

The ALEPH Collaboration

Abstract

The lifetimes of the $\bar{B}^0$ and B^- mesons have been measured with the ALEPH detector at LEP. Semileptonic decays of $\bar{B}^0$ and B^- mesons were partially reconstructed by identifying events containing a lepton with an associated D^{*+} or D^0 meson. The proper time of the B meson was estimated from the measured decay length and the momentum and mass of the D-lepton system. A fit to the proper time of 77 $D^{*+}\ell^-$ and 77 $D^0\ell^-$ candidates, combined with a constraint on the lifetime ratio (τ_-/τ_0) arising from the relative rates of observed $D^{*+}\ell^-$ and $D^0\ell^-$ events, yielded the following lifetimes:

$$\begin{aligned}
\tau_0 &= 1.52^{+0.20}_{-0.18}(\text{stat.})^{+0.07}_{-0.13}(\text{syst.})\ \text{ps} \\
\tau_- &= 1.47^{+0.22}_{-0.19}(\text{stat.})^{+0.15}_{-0.14}(\text{syst.})\ \text{ps} \\
\frac{\tau_-}{\tau_0} &= 0.96^{+0.19}_{-0.15}(\text{stat.})^{+0.18}_{-0.12}(\text{syst.})
\end{aligned}$$

(Submitted to Physics Letters B)

The ALEPH Collaboration

D. Buskulic, D. Decamp, C. Goy, J.-P. Lees, M.-N. Minard, B. Mours, B. Pietrzyk

Laboratoire de Physique des Particules (LAPP), IN^{2}P^3-CNRS, 74019 Annecy-le-Vieux Cedex, France

R. Alemany, F. Ariztizabal, P. Comas, J.M. Crespo, M. Delfino, E. Fernandez, M. Fernandez-Bosman, V. Gaitan, Ll. Garrido, T. Mattison, A. Pacheco, C. Padilla, A. Pascual

Institut de Fisica d'Altes Energies, Universitat Autonoma de Barcelona, 08193 Bellaterra (Barcelona), Spain[7]

D. Creanza, M. de Palma, A. Farilla, G. Iaselli, G. Maggi, M. Maggi, S. Natali, S. Nuzzo, M. Quattromini, A. Ranieri, G. Raso, F. Romano, F. Ruggieri, G. Selvaggi, L. Silvestris, P. Tempesta, G. Zito

INFN Sezione di Bari e Dipartimento di Fisica dell' Università, 70126 Bari, Italy

Y. Chai, H. Hu, D. Huang, X. Huang, J. Lin, T. Wang, Y. Xie, D. Xu, R. Xu, J. Zhang, L. Zhang, W. Zhao

Institute of High-Energy Physics, Academia Sinica, Beijing, The People's Republic of China[8]

L.A.T. Bauerdick,[23] E. Blucher, G. Bonvicini, J. Boudreau, D. Casper, H. Drevermann, R.W. Forty, G. Ganis, C. Gay, R. Hagelberg, J. Harvey, S. Haywood, J. Hilgart, R. Jacobsen, B. Jost, J. Knobloch, I. Lehraus, T. Lohse,[29] A. Lusiani, M. Martinez, P. Mato, H. Meinhard, A. Minten, A. Miotto, R. Miquel, H.-G. Moser, P. Palazzi, J.A. Perlas, J.-F. Pusztaszeri, F. Ranjard, G. Redlinger,[24] L. Rolandi, J. Rothberg,[2] T. Ruan, M. Saich, D. Schlatter, M. Schmelling, F. Sefkow, W. Tejessy, H. Wachsmuth, W. Wiedenmann, T. Wildish, W. Witzeling, J. Wotschack

European Laboratory for Particle Physics (CERN), 1211 Geneva 23, Switzerland

Z. Ajaltouni, F. Badaud, M. Bardadin-Otwinowska, R. El Fellous, A. Falvard, P. Gay, C. Guicheney, P. Henrard, J. Jousset, B. Michel, J-C. Montret, D. Pallin, P. Perret, F. Podlyski, J. Proriol, F. Prulhière, F. Saadi

Laboratoire de Physique Corpusculaire, Université Blaise Pascal, IN^{2}P^3-CNRS, Clermont-Ferrand, 63177 Aubière, France

T. Fearnley, J.D. Hansen, J.R. Hansen,[1] P.H. Hansen, R. Møllerud, B.S. Nilsson[1]

Niels Bohr Institute, 2100 Copenhagen, Denmark[9]

I. Efthymiopoulos, A. Kyriakis, E. Simopoulou, A. Vayaki, K. Zachariadou

Nuclear Research Center Demokritos (NRCD), Athens, Greece

J. Badier, A. Blondel, G. Bonneaud, J.C. Brient, G. Fouque, S. Orteu, A. Rougé, M. Rumpf, R. Tanaka, M. Verderi, H. Videau

Laboratoire de Physique Nucléaire et des Hautes Energies, Ecole Polytechnique, IN^{2}P^3-CNRS, 91128 Palaiseau Cedex, France

D.J. Candlin, M.I. Parsons, E. Veitch

Department of Physics, University of Edinburgh, Edinburgh EH9 3JZ, United Kingdom[10]

L. Moneta, G. Parrini

Dipartimento di Fisica, Università di Firenze, INFN Sezione di Firenze, 50125 Firenze, Italy

M. Corden, C. Georgiopoulos, M. Ikeda, J. Lannutti, D. Levinthal,[15] M. Mermikides†, L. Sawyer, S. Wasserbaech

Supercomputer Computations Research Institute and Dept. of Physics, Florida State University, Tallahassee, FL 32306, USA [12,13,14]

A. Antonelli, R. Baldini, G. Bencivenni, G. Bologna,[4] F. Bossi, P. Campana, G. Capon, F. Cerutti, V. Chiarella, B. D'Ettorre-Piazzoli,[25] G. Felici, P. Laurelli, G. Mannocchi,[5] F. Murtas, G.P. Murtas, L. Passalacqua, M. Pepe-Altarelli, P. Picchi[4]

Laboratori Nazionali dell'INFN (LNF-INFN), 00044 Frascati, Italy

P. Colrain, I. ten Have, J.G. Lynch, W. Maitland, W.T. Morton, C. Raine, P. Reeves, J.M. Scarr, K. Smith, M.G. Smith, A.S. Thompson, R.M. Turnbull

Department of Physics and Astronomy, University of Glasgow, Glasgow G12 8QQ,United Kingdom[10]

B. Brandl, O. Braun, C. Geweniger, P. Hanke, V. Hepp, E.E. Kluge, Y. Maumary, A. Putzer, B. Rensch, A. Stahl, K. Tittel, M. Wunsch

Institut für Hochenergiephysik, Universität Heidelberg, 6900 Heidelberg, Fed. Rep. of Germany[16]

A.T. Belk, R. Beuselinck, D.M. Binnie, W. Cameron, M. Cattaneo, D.J. Colling, P.J. Dornan, S. Dugeay, A.M. Greene, J.F. Hassard, N.M. Lieske,[31] J. Nash, D.G. Payne, M.J. Phillips, J.K. Sedgbeer, I.R. Tomalin, A.G. Wright

Department of Physics, Imperial College, London SW7 2BZ, United Kingdom[10]

P. Girtler, E. Kneringer, D. Kuhn, G. Rudolph

Institut für Experimentalphysik, Universität Innsbruck, 6020 Innsbruck, Austria[18]

C.K. Bowdery, T.J. Brodbeck, A.J. Finch, F. Foster, G. Hughes, D. Jackson, N.R. Keemer, M. Nuttall, A. Patel, T. Sloan, S.W. Snow, E.P. Whelan

Department of Physics, University of Lancaster, Lancaster LA1 4YB, United Kingdom[10]

K. Kleinknecht, J. Raab, B. Renk, H.-G. Sander, H. Schmidt, F. Steeg, S.M. Walther, R. Wanke, B. Wolf

Institut für Physik, Universität Mainz, 6500 Mainz, Fed. Rep. of Germany[16]

J-J. Aubert, A.M. Bencheikh, C. Benchouk, A. Bonissent, J. Carr, P. Coyle, J. Drinkard,[3] F. Etienne, D. Nicod, S. Papalexiou, P. Payre, L. Roos, D. Rousseau, P. Schwemling, M. Talby

Centre de Physique des Particules, Faculté des Sciences de Luminy, IN^{2}P^3-CNRS, 13288 Marseille, France

S. Adlung, R. Assmann, C. Bauer, W. Blum, D. Brown, P. Cattaneo,[28] B. Dehning, H. Dietl, F. Dydak,[22] M. Frank, A.W. Halley, J. Lauber, G. Lütjens, G. Lutz, W. Männer, R. Richter, H. Rotscheidt, J. Schröder, A.S. Schwarz, R. Settles, H. Seywerd, U. Stierlin, U. Stiegler, R. St. Denis, G. Wolf

Max-Planck-Institut für Physik, Werner-Heisenberg-Institut, 8000 München, Fed. Rep. of Germany[16]

J. Boucrot,[1] O. Callot, A. Cordier, M. Davier, L. Duflot, J.-F. Grivaz, Ph. Heusse, D.E. Jaffe, P. Janot, D.W. Kim,[19] F. Le Diberder, J. Lefrançois, A.-M. Lutz, M.-H. Schune, J.-J. Veillet, I. Videau, Z. Zhang,

Laboratoire de l'Accélérateur Linéaire, Université de Paris-Sud, IN^{2}P^3-CNRS, 91405 Orsay Cedex, France

D. Abbaneo, G. Bagliesi, G. Batignani, L. Bosisio, U. Bottigli, C. Bozzi, G. Calderini, M. Carpinelli, M.A. Ciocci, R. Dell'Orso, I. Ferrante, F. Fidecaro, L. Foà, E. Focardi, F. Forti, A. Giassi, M.A. Giorgi, A. Gregorio, F. Ligabue, E.B. Mannelli, P.S. Marrocchesi, A. Messineo, F. Palla, G. Rizzo, G. Sanguinetti, P. Spagnolo, J. Steinberger, R. Tenchini, G. Tonelli, G. Triggiani, C. Vannini, A. Venturi, P.G. Verdini, J. Walsh

Dipartimento di Fisica dell'Università, INFN Sezione di Pisa, e Scuola Normale Superiore, 56010 Pisa, Italy

A.P. Betteridge, J.M. Carter, M.G. Green, P.V. March, Ll.M. Mir, T. Medcalf, I.S. Quazi, J.A. Strong, L.R. West

Department of Physics, Royal Holloway & Bedford New College, University of London, Surrey TW20 OEX, United Kingdom[10]

D.R. Botterill, R.W. Clifft, T.R. Edgecock, M. Edwards, S.M. Fisher, T.J. Jones, P.R. Norton, D.P. Salmon, J.C. Thompson

Particle Physics Dept., Rutherford Appleton Laboratory, Chilton, Didcot, Oxon OX11 OQX, United Kingdom[10]

B. Bloch-Devaux, P. Colas, H. Duarte, W. Kozanecki, E. Lançon, M.C. Lemaire, E. Locci, P. Perez, F. Perrier, J. Rander, J.-F. Renardy, A. Rosowsky, A. Roussarie, J.-P. Schuller, J. Schwindling, D. Si Mohand, B. Vallage

Service de Physique des Particules, DAPNIA, CE-Saclay, 91191 Gif-sur-Yvette Cedex, France[17]

R.P. Johnson, A.M. Litke, G. Taylor, J. Wear

Institute for Particle Physics, University of California at Santa Cruz, Santa Cruz, CA 95064, USA[27]

J.G. Ashman, W. Babbage, C.N. Booth, C. Buttar, R.E. Carney, S. Cartwright, F. Combley, F. Hatfield, L.F. Thompson[1]

Department of Physics, University of Sheffield, Sheffield S3 7RH, United Kingdom[10]

E. Barberio, A. Böhrer, S. Brandt, G. Cowan, C. Grupen, G. Lutters, F. Rivera,[32] U. Schäfer, L. Smolik

Fachbereich Physik, Universität Siegen, 5900 Siegen, Fed. Rep. of Germany[16]

R. Della Marina, G. Giannini, B. Gobbo, F. Ragusa[21]

Dipartimento di Fisica, Università di Trieste e INFN Sezione di Trieste, 34127 Trieste, Italy

L. Bellantoni, W. Chen, D. Cinabro,[26] J.S. Conway,[30] D.F. Cowen,[20] Z. Feng, D.P.S. Ferguson, Y.S. Gao, J. Grahl, J.L. Harton, R.C. Jared,[6] B.W. LeClaire, C. Lishka, Y.B. Pan, J.R. Pater, Y. Saadi, V. Sharma, M. Schmitt, Z.H. Shi, A.M. Walsh, F.V. Weber, Sau Lan Wu, X. Wu, M. Zheng, G. Zobernig

Department of Physics, University of Wisconsin, Madison, WI 53706, USA[11]

---

†Deceased.

[1]Now at CERN, PPE Division, 1211 Geneva 23, Switzerland.

[2]Permanent address: University of Washington, Seattle, WA 98195, USA.

[3]Now at University of California, Irvine, CA 92717, USA.

[4]Also Istituto di Fisica Generale, Università di Torino, Torino, Italy.

[5]Also Istituto di Cosmo-Geofisica del C.N.R., Torino, Italy.

[6]Permanent address: LBL, Berkeley, CA 94720, USA.

[7]Supported by CICYT, Spain.

[8]Supported by the National Science Foundation of China.

[9]Supported by the Danish Natural Science Research Council.

[10]Supported by the UK Science and Engineering Research Council.

[11]Supported by the US Department of Energy, contract DE-AC02-76ER00881.

[12]Supported by the US Department of Energy, contract DE-FG05-87ER40319.

[13]Supported by the NSF, contract PHY-8451274.

[14]Supported by the US Department of Energy, contract DE-FC0S-85ER250000.

[15]Supported by SLOAN fellowship, contract BR 2703.

[16]Supported by the Bundesministerium für Forschung und Technologie, Fed. Rep. of Germany.

[17]Supported by the Direction des Sciences de la Matière, C.E.A.

[18]Supported by Fonds zur Förderung der wissenschaftlichen Forschung, Austria.

[19]Supported by the Korean Science and Engineering Foundation and Ministry of Education.

[20]Now at California Institute of Technology, Pasadena, CA 91125, USA.

[21]Now at Dipartimento di Fisica, Università di Milano, Milano, Italy.

[22]Also at CERN, PPE Division, 1211 Geneva 23, Switzerland.

[23]Now at DESY, Hamburg, Germany.

[24]Now at TRIUMF, Vancouver, B.C., Canada.

[25]Also at Università di Napoli, Dipartimento di Scienze Fisiche, Napoli, Italy.

[26]Now at Harvard University, Cambridge, MA 02138, U.S.A.

[27]Supported by the US Department of Energy, grant DE-FG03-92ER40689.

[28]Now at Università di Pavia, Pavia, Italy.

[29]Now at Max-Planck-Institut f. Kernphysik, Heidelberg, Germany.

[30]Now at Rutgers University, Piscataway, NJ 08854, USA.

[31]Now at Oxford University, Oxford OX1 3RH, U.K.

[32]Partially supported by Colciencias, Colombia.

1 Introduction

Recent experimental improvements have resulted in precise measurements of the average B hadron lifetime [1, 2], but measurements of the lifetimes of the individual B species are less precise [3]. Indirect measurements of the ratio of the $\bar{B}^0$ and B^- lifetimes have been made as well [4, 5].

Knowledge of the ratio of the $\bar{B}^0$ and B^- lifetimes is relevant for a quantitative understanding of the importance of non-spectator effects and final state interactions in B meson decays. Such effects are large in the charm sector (where $\tau_{D^+}/\tau_{D^0} \simeq 2.5$), but are predicted to be much smaller for B decays [6].

This Letter reports a measurement of the $\bar{B}^0$ and B^- lifetimes with the ALEPH detector at LEP. Semileptonic decays of $\bar{B}^0$ and B^- mesons were partially reconstructed by identifying events containing a lepton (e or μ) with an associated D^0 or D^{*+} meson. The resulting D^0-lepton ($D^0\ell^-$) and D^{*+}-lepton ($D^{*+}\ell^-$) event samples consist mostly of B^- and $\bar{B}^0$ decays, respectively (charge conjugate modes are implied throughout this Letter). The separation of B meson species in this manner allows a measurement of their individual lifetimes.

2 The ALEPH detector

The ALEPH detector is described in detail elsewhere [7]. A high resolution vertex detector (VDET) consisting of two layers of silicon with double-sided readout was available for this analysis. It provides measurements in the $r\phi$ and z directions at radii of 6.3 cm and 10.8 cm, with $\simeq$ 12 μm precision. The VDET provides full azimuthal coverage and polar angle coverage to $|\cos\theta| < 0.85$ for the inner layer only and $|\cos\theta| < 0.69$ for both layers [8]. Outside VDET particles traverse the inner tracking chamber (ITC) and the time projection chamber (TPC). The ITC is a cylindrical drift chamber with eight axial wire layers at radii of 16 to 26 cm. The TPC measures up to 21 space points per track at radii between 40 and 171 cm, and also provides up to 330 measurements of the ionization (dE/dx) of each charged track. Tracking is performed in a 1.5 T magnetic field provided by a superconducting solenoid.

The electromagnetic calorimeter (ECAL) is a lead/wire-chamber sandwich operated in proportional mode. The calorimeter is read out in projective towers that subtend typically 15 mrad $\times$ 15 mrad in solid angle and that are segmented in three longitudinal sections. The hadron calorimeter (HCAL) uses the iron return yoke as absorber. Hadronic showers are sampled by 23 planes of streamer tubes, with analog projective tower and digital hit pattern readout. The HCAL is used in combination with two layers of muon chambers outside the magnet for muon identification.

3 Event selection

The $D^{*+}\ell^-$ and $D^0\ell^-$ event samples were selected from approximately 260,000 hadronic decays of the Z, collected in 1991 when the VDET became fully operational.

Hadronic event selection based on charged tracks is described in ref. [9].

The selection of muons and electrons is described in detail in ref. [10]. For this analysis, lepton candidates were required to have a momentum of at least 3 GeV/c. Electron candidates that had suffered a hard bremstrahlung due to interaction with detector material have been removed using the technique described in ref. [11].

D^{*+} and D^0 candidates were reconstructed from charged tracks that formed an angle of less than 45° with the lepton candidate. These charged tracks were also required to intersect an imaginary cylinder of radius 2 cm and half-length 4 cm centered on the nominal interaction point, have at least 4 hits in the TPC, have a polar angle θ such that $|\cos\theta| < 0.95$ and have momentum greater than 200 MeV/c.

D^{*+} candidates were identified via the decay $D^{*+} \to D^0\pi^+$, followed either by $D^0 \to K^-\pi^+$ or $D^0 \to K^-\pi^+\pi^-\pi^+$. It is well known that the very low Q value for the decay $D^{*+} \to D^0\pi^+$ permits the identification of D^{*+} mesons with low background (a detailed presentation of inclusive D^{*+} selection is given in ref. [12]). In this analysis, the favorable kinematic situation was exploited by requiring that the difference in mass between the D^{*+} and D^0 candidates lie within 1.5 MeV/c^2 (approximately two standard deviations of the experimental resolution) of the known value of 145.6 MeV/c^2. Since, for these decays, the kaon will have the same electric charge as the lepton coming from the semileptonic decay of the B, this charge correlation was imposed in the reconstruction of D^{*+} mesons. For the subsample where $D^0 \to K^-\pi^+$ the momentum of the D^0 was required to be greater than 5 GeV/c. The subsample with $D^0 \to K^-\pi^+\pi^-\pi^+$ suffers from greater combinatorial background and therefore the following more stringent selection criteria were applied: $p_{D^0} > 8$ GeV/c; if there are at least 40 dE/dx wire samples for the K track, its specific ionization must be within two standard deviations of that expected for a kaon; and at least two of the D^0 decay tracks have $p > 1$ GeV/c. If, for a given detected lepton, more than one combination satisfied these selection criteria, the best combination was selected, based on the values of the reconstructed D^0 mass and D^{*+}–D^0 mass difference.

The $D^0\ell^-$ sample consists of events with a lepton and a D^0 candidate, where the D^0 was not the decay product of a D^{*+}. D^0 candidates were identified via the decay $D^0 \to K^-\pi^+$. Again, K candidates were required to have the same charge as the lepton. For this sample, the powerful selection criterion involving the D^{*+}–D^0 mass difference was not applicable, making it necessary to apply stricter selection criteria. The D^0 candidates were required to have $p_{D^0} > 8$ GeV/c, $p_K > 2$ GeV/c and $p_\pi > 1.5$ GeV/c. Furthermore, the specific ionization of both tracks, if at least 40 wire samples had been recorded, had to be within 2σ of that expected of a kaon and a pion, respectively. To reject D^0 candidates coming from $D^{*+} \to D^0\pi^+$, a search for the additional pion was performed. If a pion candidate yielding a D^{*+}–D^0 mass difference within 1.5 MeV/c^2 of the known value was found, the $D^0\ell^-$ candidate was rejected. The efficiency for reconstructing the additional pion and rejecting D^0's coming from D^{*+} decays was found to be 85%.

To improve the signal to background ratio and to ensure well-measured decay lengths, additional selection criteria were placed on all the subsamples. The invariant mass of the $D^{(*)}\ell$ (where $D^{(*)}$ can be D^{*+} or D^0) system was required to be greater

Table 1: Fitted D^0 mass and number of D^0 candidates and background events falling within a mass window of $\pm 2\sigma$.

Subsample		Mass (MeV/c^2)	Signal events	Background events
$D^{*+}\ell^-$	$D^0 \to K^-\pi^+$	1866 ± 2	28.4 ± 5.4	2.2 ± 1.1
	$D^0 \to K^-\pi^+\pi^-\pi^+$	1864 ± 2	40.7 ± 7.2	6.7 ± 4.0
$D^0\ell^-$	$D^0 \to K^-\pi^+$	1864 ± 2	65.9 ± 8.8	11.7 ± 4.0

than 3 GeV/c^2. This criterion significantly reduced the combinatorial background, while keeping $\sim 85\%$ of the signal [13]. To exploit the high precision of the silicon vertex detector, the lepton track and the D^0 decay product tracks were required to have at least one VDET hit in both the $r\phi$ and z projections (except for the decay $D^0 \to K^-\pi^+\pi^-\pi^+$, where at least two of the four tracks were required to have VDET hits). Also, the D and B decay vertices were reconstructed (as will be discussed in Sec. 4) and the χ^2 probability for each vertex fit was required to be greater than 1%.

The D^0 candidate mass spectra for the three subsamples are shown in Fig. 1. For $D^0 \to K^-\pi^+$ the fitted curves consist of a Gaussian for the signal plus a linear background. The width of the Gaussian was fixed at 10 MeV/c^2, determined from a Monte Carlo simulation.

For $D^0 \to K^-\pi^+\pi^-\pi^+$ the use of the D^0 mass as one of the criteria to select the best among several candidates for a given event causes the background to exhibit a broad peak centered on the D^0 mass. A Gaussian, whose area and width were determined by considering the D^0 mass spectrum for events that fail the D^{*+}–D^0 mass difference criterion, was combined with a straight line to describe this background. The signal was described by a Gaussian with the width fixed at 9 MeV/c^2.

The fitted D^0 mass and the fitted number of signal and background events within a window of $\pm 2\sigma$ around the fitted mass for the three samples are shown in Tab. 1.

4 Decay length and proper time

Events reconstructed with a D^0 mass within two standard deviations of the fitted D^0 mass were selected for the lifetime analysis, resulting in 77 $D^{*+}\ell^-$ and 77 $D^0\ell^-$ candidates. The decay length has been calculated for these events by reconstructing the primary and B decay vertices in three dimensions.

The primary vertex reconstruction algorithm combines the average beam position, determined from data for each run, with the track information from the particular event. After grouping the tracks into jets, tracks within each particular jet were projected into the plane perpendicular to the jet direction. This removes any dependence on the lifetime of the particle in the approximation that the jet axis

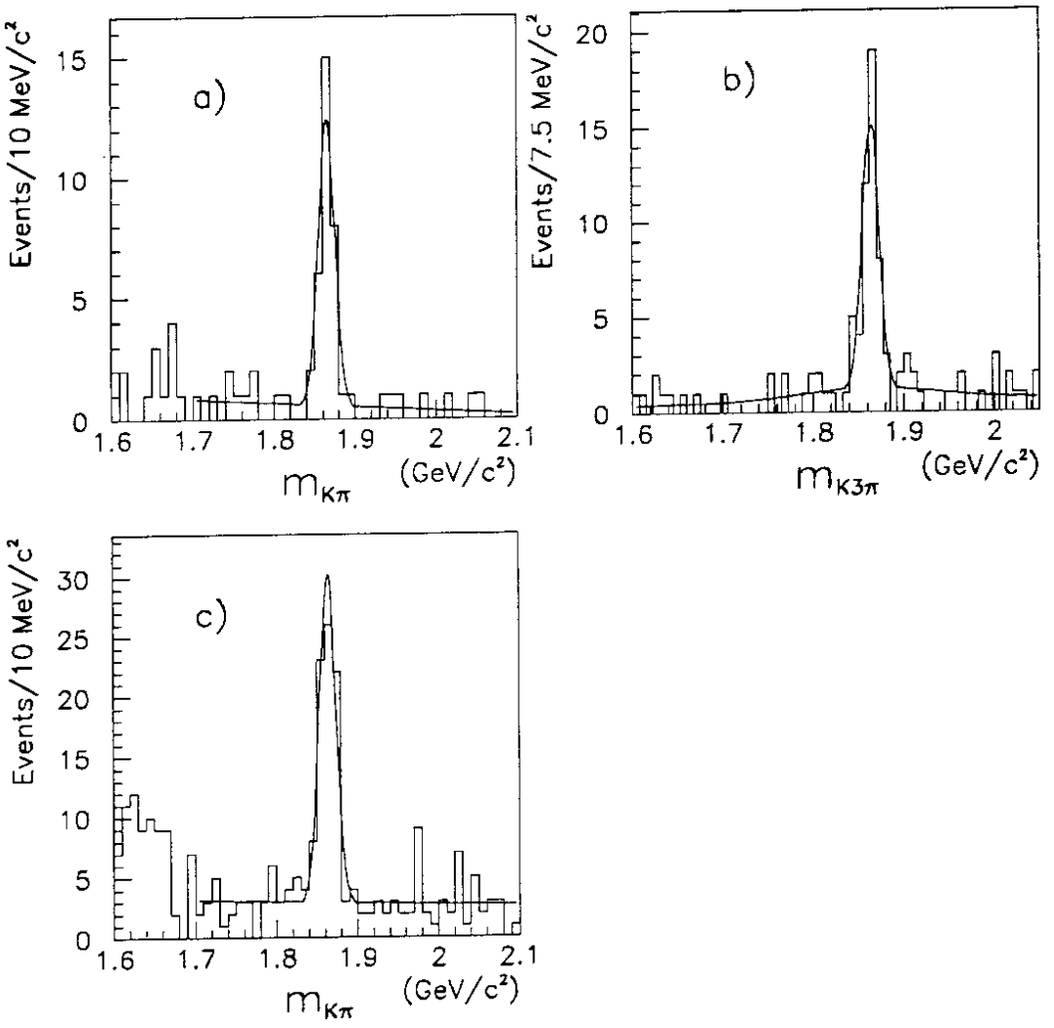

Figure 1: The invariant mass of D^0 candidates for the three subsamples: a) $D^{*+}\ell^-$, $D^0 \to K\pi$, b) $D^{*+}\ell^-$, $D^0 \to K3\pi$, c) $D^0\ell^-$, $D^0 \to K\pi$. The smooth curves are results of the fit described in the text. The mass region below 1.7 GeV/c^2 is excluded from the fit for the $D^0 \to K^-\pi^+$ samples to avoid a broad peak arising from the decay $D^0 \to K^-\pi^+\pi^0$ where the π^0 goes undetected.

reproduces the direction of the b hadron. The primary vertex was then calculated as the point that was most consistent with the projected tracks and the beam envelope, which was taken as the average beam position with the dimensions of the LEP beam spot ($\sim$ 150 μm $\times$ 10 μm $\times$ 1 cm). Using this algorithm on simulated $b\bar{b}$ events, an average resolution of the primary vertex position projected along the event sphericity axis of 85 μm is obtained.

The B decay vertex was obtained by first reconstructing the D^0 decay vertex using its known decay tracks and then extrapolating the neutral D^0 track backwards where it was combined with the lepton to form the B decay vertex (Fig. 2). In the case of $D^{*+}\ell^-$ events, the soft pion from the D^{*+} decay does not improve the

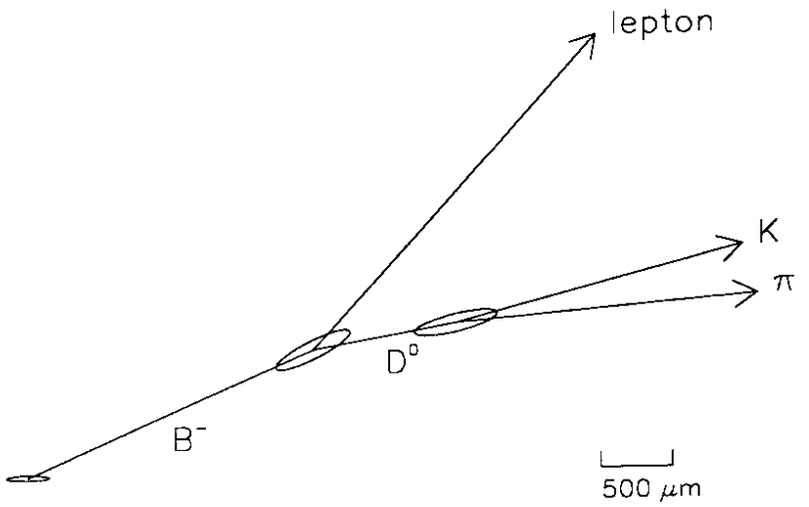

Figure 2: Schematic representation of a typical B decay into $D^0\ell^-$.

resolution on the B decay length and was therefore not used in the reconstruction of the B vertex.

The best estimates of the B decay length δ and its error σ_δ are obtained by combining the reconstructed primary and secondary vertices with the B flight direction, using the formulas

$$\delta = \sum_{i,j} \frac{n_i \sigma_{ij}^{-1} x_j}{n_i \sigma_{ij}^{-1} n_j} \qquad \sigma_\delta^2 = \sum_{i,j} \frac{1}{n_i \sigma_{ij}^{-1} n_j} \tag{1}$$

where x_i is the vector that points from the primary vertex position to the B decay vertex position, n_i is the vector of direction cosines of the B flight direction, and σ_{ij}^{-1} is the inverse of the sum of the error matrices of the primary and B vertices. The uncertainty on the flight direction due to the missing neutrino induces a negligible error on the decay length. The resolution on the B decay length is typically about 300 μm, compared with an average B decay length of $\sim$ 2.6 mm (assuming τ_b = 1.49 ps and an average B momentum of 30 GeV/c).

The proper time for a decay is the decay length divided by $\beta\gamma c = p/m$, however since these events contain an undetected neutrino, the B momentum is not known. A good approximation to the proper time t is obtained by using the $D^{(*)}\ell$ system when evaluating $\beta\gamma$,

$$t = \frac{\delta}{(\beta\gamma c)_{D\ell}}, \qquad \sigma_t = \frac{\sigma_\delta}{(\beta\gamma c)_{D\ell}}. \tag{2}$$

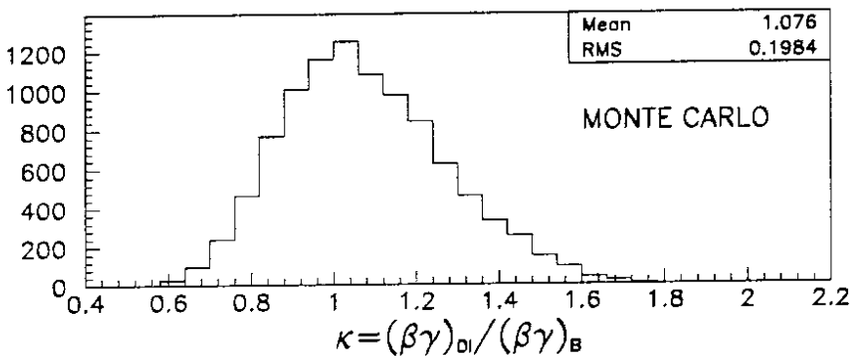

Figure 3: Distribution of κ (defined in the text).

Then κ is defined as

$$\kappa = \frac{(\beta\gamma)_{D\ell}}{(\beta\gamma)_B}. \tag{3}$$

A typical distribution of κ for Monte Carlo signal events is shown in Fig. 3. To perform a maximum likelihood fit for the lifetimes it is necessary to compute for each event the probability of observing a proper time t (as obtained from Eq. 2) given the lifetime τ. The probability function $F(t, \sigma_t, \tau)$ is obtained by convoluting an exponential distribution with the properly normalised κ distribution. Since this distribution depends on the selection criteria applied, separate κ distributions are calculated for each subsample.

Due to the finite resolution on the decay length (and hence on the proper time) it is necessary to perform a second convolution with a Gaussian resolution function. It has been determined from a Monte Carlo simulation that the resolution on the proper time is best described by the sum of two Gaussians, where the widths of the Gaussians are given by σ_t multiplied by a scale factor:

$$R_{res}(t - t_0, \sigma_t) = \frac{1 - A_2}{\sqrt{2\pi}c_1\sigma_t} \exp\left[-\frac{(t-t_0)^2}{2\,(c_1\sigma_t)^2}\right] + \frac{A_2}{\sqrt{2\pi}c_2\sigma_t} \exp\left[-\frac{(t-t_0)^2}{2\,(c_2\sigma_t)^2}\right], \tag{4}$$

with parameters $c_1 = 1.12 \pm 0.06$, $c_2 = 2.66 \pm 0.42$ and $A_2 = 0.24 \pm 0.05$. The second term in Eq. 4 is necessary to model small non-Gaussian effects in the reconstruction of charged tracks. Due to the good resolution on proper time, the fitted lifetimes are rather insensitive to the precise values of c_1, c_2, and A_2.

Summarizing, the probability distribution that describes the signal is obtained by convoluting an exponential decay function with the κ distribution of Fig. 3 and the resolution function of Eq. 4.

5 $\bar{B}^0$ and B^- lifetimes

The $\bar{B}^0$ and B^- lifetimes cannot be determined by performing separate fits on the two event samples. Since both samples contain a mixture of $\bar{B}^0$ and B^- decays, one

does not expect their distributions to be described by a single exponential. Furthermore, the $B^-/\bar{B}^0$ mixture in the samples depends on the ratio of the lifetimes, as will be discussed below. Therefore, to measure the $\bar{B}^0$ and B^- lifetimes a simultaneous maximum likelihood fit to all the events was performed. Since each of the two samples contains a mixture of $\bar{B}^0$ and B^- decays and of background, the likelihood function contains three components for each sample. The likelihood function is written as

$$\begin{aligned} \mathcal{L}_0 &= \prod_{i=1}^{N_{D^{*}\ell}} f_-^* F(t_i,\sigma_i,\tau_-) + f_0^* F(t_i,\sigma_i,\tau_0) + f_{BG}^* F_{BG}^*(t_i) \\ &\times \prod_{i=1}^{N_{D^0\ell}} f_-^0 F(t_i,\sigma_i,\tau_-) + f_0^0 F(t_i,\sigma_i,\tau_0) + f_{BG}^0 F_{BG}^0(t_i) \end{aligned} \tag{5}$$

where $F(t,\sigma,\tau)$ is the probability function for the signal, as described in the previous section. The coefficients f_-^* and f_0^* are the fractions of the $D^{*+}\ell^-$ sample arising from B^- and $\bar{B}^0$ decays, respectively. Similarly, f_-^0 and f_0^0 are the fractions of the $D^0\ell^-$ sample made up of B^- and $\bar{B}^0$ decays. The coefficients f_{BG}^* and f_{BG}^0 are the background fractions of the samples, while the functions $F_{BG}^*(t)$ and $F_{BG}^0(t)$ are their normalised proper time distributions.

5.1 Backgrounds

Background contamination arises from the following sources:

(1) combinatorial background, i.e. candidates with a fake $D^{(*)}$;

(2) the process $\bar{B} \to D_s^- D^{(*)} X$, followed by $D_s^- \to \ell^- X$, giving rise to a real $D^{(*)}$ and a real lepton;

(3) a real $D^{(*)}$ meson accompanied by a fake or non-prompt lepton, from $Z \to b\bar{b}$ or $Z \to c\bar{c}$ events.

Source (1) is the dominant background and its contribution is determined from a fit to the D^0 mass distributions, and its magnitude is given in Tab. 1 for the various subsamples. The proper time distribution for this source has been determined from the data by selecting events from the sidebands of the D^0 peak. The same selection criteria described in Sec. 3 have been applied to the background samples, except that the requirement on the D^{*+}–D^0 mass difference in the case of the $D^{*+}\ell^-$ events has been removed to increase the statistics. A function consisting of a Gaussian plus positive and negative exponential tails was used to describe these data (Fig. 4a–c.)

The contribution from source (2) was calculated from the measured branching ratios for this process [14] plus a Monte Carlo simulation to determine the detection efficiency. The proper time distribution for this source was determined from the simulation and is well approximated by an exponential distribution with the mean b hadron lifetime, $\tau_b = 1.49 \pm 0.07$ ps [2].

The background from source (3) is estimated from the known hadron-lepton misidentification probabilities and the measured inclusive D^0 and D^{*+} rates. It can be further subdivided into three distinct components,

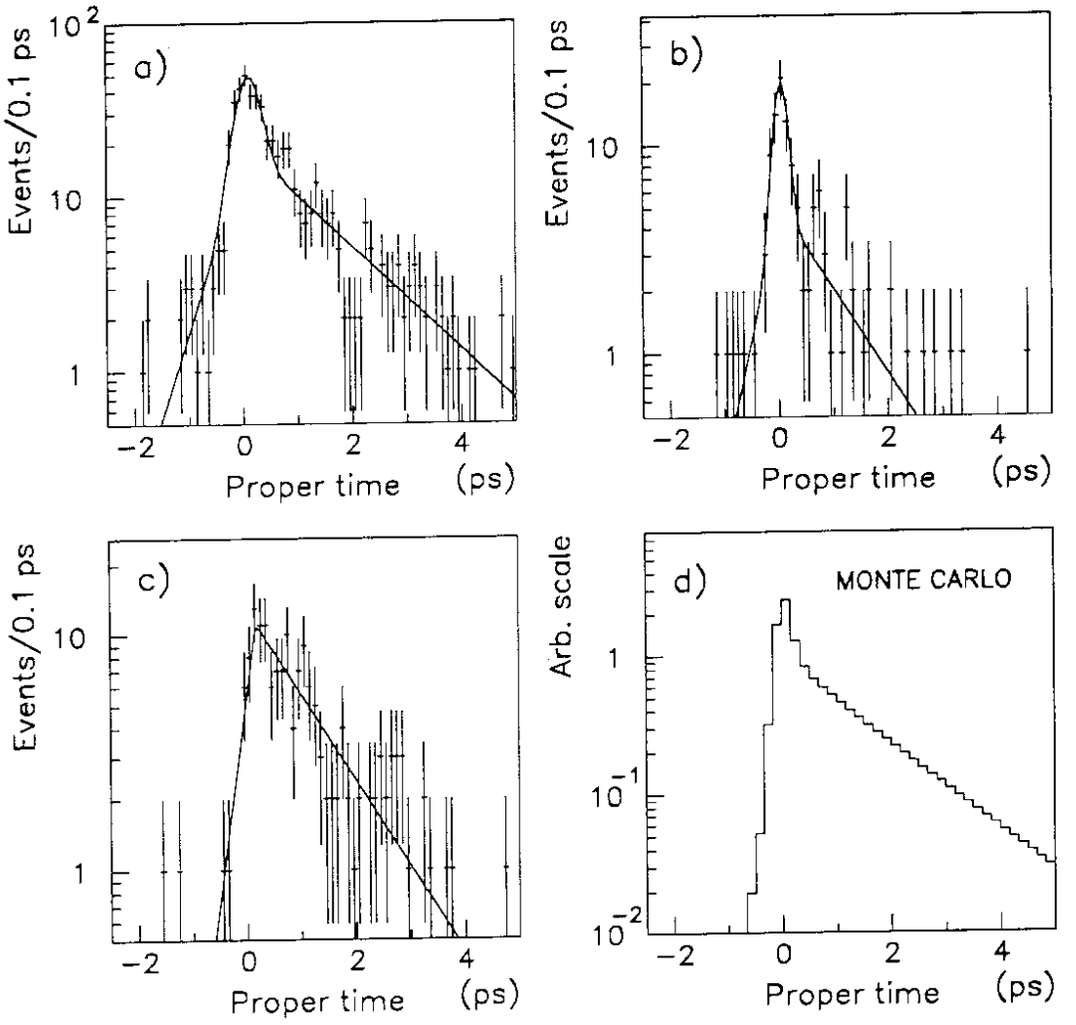

Figure 4: Proper time distributions for the three different samples for background due to source (1), a) $D^{*+}\ell^-$, $D^0 \to K\pi$, b) $D^{*+}\ell^-$, $D^0 \to K3\pi$, c) $D^0\ell^-$, $D^0 \to K\pi$. The smooth curves are results of the fit described in the text. d) shows the proper time distribution for events arising from background sources (2) and (3), as obtained from a Monte Carlo simulation.

- $c\bar{c}$ events where the fake lepton comes from the primary vertex,
- $b\bar{b}$ events where the fake lepton comes from the primary vertex, and
- $b\bar{b}$ events where the fake lepton comes from the decaying b hadron.

The distribution of background source (3) in these three components and their proper time distributions have been determined from a Monte Carlo simulation. The proper time distribution for the sum of sources (2) and (3) for the $D^{*+}\ell^-$, $D^0 \to K^-\pi^+$ subsample is shown in Fig. 4d. The corresponding distributions for the other event samples are similar.

Table 2: Background sources and their contributions (in number of events) to the three subsamples.

Subsample		Combinatorial	Fake lepton	$\bar{B} \to D_s^- D^{(*)} X$
$D^{*+}\ell^-$	$D^0 \to K^-\pi^+$	2.2 ± 1.1	0.9 ± 0.3	0.7 ± 0.3
	$D^0 \to K^-\pi^+\pi^-\pi^+$	6.7 ± 4.0	1.5 ± 0.5	1.0 ± 0.4
$D^0\ell^-$	$D^0 \to K^-\pi^+$	11.7 ± 4.0	1.9 ± 0.7	1.9 ± 0.7

The estimated number of events due to each background source for the different subsamples is shown in Tab. 2.

5.2 Sample compositions

Each of the two event samples contains a mixture of $\bar{B}^0$ and B^- decays, and the sample compositions (the coefficients f_-^*, f_0^*, f_-^0 and f_0^0 of Eq. 5) must be calculated to complete the specification of the likelihood function. The difficulty in evaluating the sample compositions arises from incomplete knowledge of the branching ratios of certain decay modes that contribute to the two samples. In particular, the branching ratios for decays of the type[1] $\bar{B} \to D^{(*)}\pi\ell\nu$ have not been measured. This type of decay is important because it contributes to the amount of B meson of the "wrong" species in the two samples.

The $\bar{B}^0$ and B^- content of the two samples were calculated using the following method: the relevant semileptonic branching ratios for $\bar{B}^0$ mesons were taken from measurements at the $\Upsilon(4S)$ energy. Where measurements were incomplete, reasonable assumptions based on isospin conservation were applied. The B^- branching fractions were then obtained from

$$B(B^- \to \ell^- X) = \frac{\tau_-}{\tau_0} B(\bar{B}^0 \to \ell^- X') \tag{6}$$

which derives from the expectation that the partial semileptonic decay widths are equal. The sample coefficients were then calculated by considering the $\bar{B}^0$ and B^- decay channels that contribute to the $D^{*+}\ell^-$ and $D^0\ell^-$ samples. As a consequence of this procedure, the coefficients f_-^*, f_0^*, f_-^0 and f_0^0 appearing in the likelihood function (Eq. 5) depend on the lifetime ratio. The full calculation, given in detail in the Appendix, shows that the $D^{*+}\ell^-$ sample contains mostly $\bar{B}^0$ decays and the $D^0\ell^-$ sample mostly B^-. For example, if the lifetimes were equal, one would obtain $f_0^* = 0.73$ and $f_-^* = 0.10$ for the $D^{*+}\ell^-$ sample and $f_-^0 = 0.64$ and $f_0^0 = 0.20$ for the $D^0\ell^-$ sample.

The technique of taking only the measured $\bar{B}^0$ branching fractions and calculating the B^- branching fractions using Eq. 6 prevents the introduction of a lifetime bias into the measurement, as would be the case, for example, if both the $\bar{B}^0$ and B^- branching fractions were taken from previous measurements.

[1] $\bar{B} \to D^{(*)}\pi\ell\nu$ is used to denote decays with non-resonant π production as well as decays of the type $\bar{B} \to D^{**}\ell\nu$.

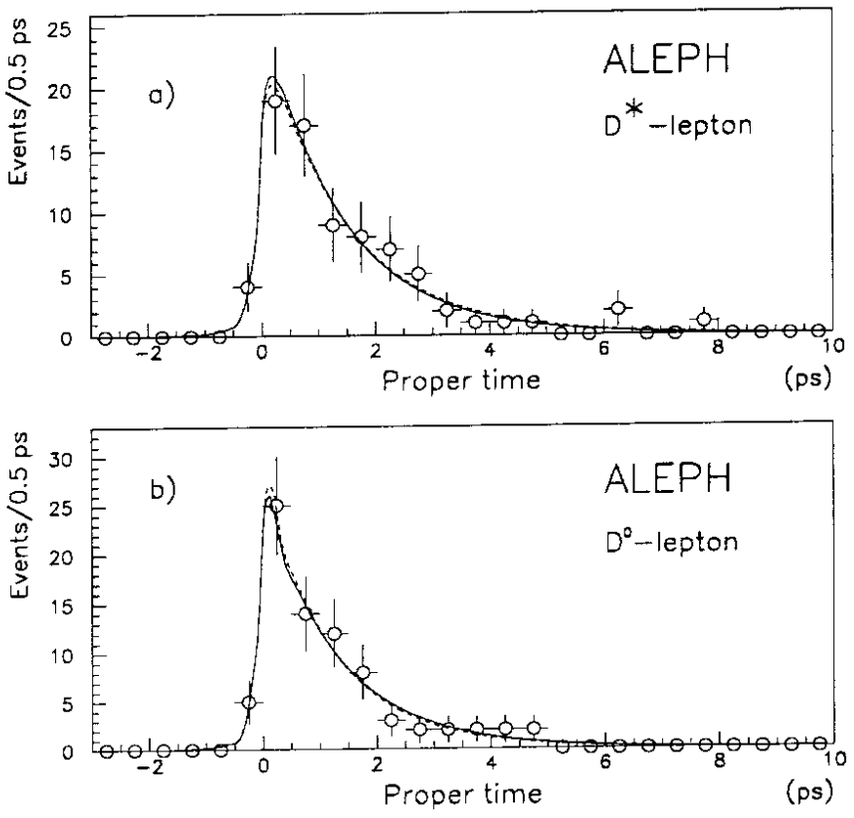

Figure 5: Proper time distributions with result of the fit overlaid for the two samples, a) $D^{*+}\ell^-$ events, b) $D^0\ell^-$ events. The solid curve shows the result of the full fit, including the event ratio constraint. The dashed curve corresponds to the fit without the event ratio information.

5.3 Fit results

A maximum likelihood fit to the proper time distributions of the $D^{*+}\ell^-$ and $D^0\ell^-$ events was performed to determine the two free parameters τ_0 and τ_-. The resulting lifetime values are

$$\begin{aligned} \tau_0 &= 1.64^{+0.25}_{-0.23}(\text{stat.})^{+0.06}_{-0.05}(\text{syst.})\ \text{ps} \\ \tau_- &= 1.30^{+0.28}_{-0.27}(\text{stat.}) \pm 0.06(\text{syst.})\ \text{ps} \end{aligned}$$

where the sources of systematic error are discussed in Sec. 6. The two lifetimes are consistent with the average b hadron lifetime and the ratio of the lifetimes is consistent with unity. The proper time distributions for the two samples are shown in Fig. 5, with the results of the fit overlaid (dashed curve).

As a check on the procedure, a measurement of the D^0 lifetime has been performed. The D^0 flight distance is calculated as the distance between the B and D^0 decay vertices. An unbinned likelihood fit to the 154 events yields

$$\tau_{D^0} = 0.39 \pm 0.04(\text{stat.})\ \text{ps}$$

in good agreement with the world average value $\tau_{D^0} = 0.420 \pm 0.008$ ps [16].

5.4 Event ratio constraint

The statistical precision of the lifetime measurement can be enhanced significantly if the relative rates of $D^{*+}\ell^-$ and $D^0\ell^-$ events are taken into consideration. As for the sample compositions, the expected ratio of the number of $D^{*+}\ell^-$ events to the number of $D^0\ell^-$ events (R) is a function of the lifetime ratio, via Eq. 6. The dependence of R on the lifetime ratio was used with the observed ratio (R_{obs}) to add a further constraint in the fit.

To measure R_{obs} with greater statistical precision, the selection criteria requiring VDET hits and good vertex probabilities have been removed. This resulted in an increase of $\sim 40\%$ in the event samples. The observed event ratio was found to be

$$R_{obs} = 1.02 \pm 0.17 \pm 0.05.$$

The systematic error arises from uncertainty in the fitting of the D^0 mass peak and in the background subtraction.

The expected ratio R was calculated as a function of the lifetime ratio using the $\bar{B}^0$ semileptonic branching fractions in a manner similar to that used in the calculation of the sample compositions. The D^0 branching ratios for the channels selected and the selection efficiency for each channel were also necessary to calculate R. It was assumed that equal numbers of $\bar{B}^0$ and B^- mesons are produced in Z decays. This is a reasonable assumption since B^* mesons decay only by emitting a photon, and the B^{**}–B mass difference is expected to lie well above the pion mass [15]. Figure 6 shows a plot of the quantity R with its 1σ error versus the lifetime ratio τ_-/τ_0. The principal error arises from uncertainty in the breakdown of $\bar{B}^0$ semileptonic branching fractions. One can see from the plot that a value of the lifetime ratio of $\tau_-/\tau_0 \sim 1$ is preferred, and in fact, using this event ratio information alone, one obtains

$$\frac{\tau_-}{\tau_0} = 1.12^{+0.37}_{-0.24}(\text{stat}). \tag{7}$$

The statistical error here comes from the error on R_{obs}. The error due to the spread of the curves is a systematic error which will be considered when evaluating the systematic uncertainty on the fitted lifetimes.

The information on the event ratio was combined with the decay length information in a coherent way by multiplying the likelihood function by the probability of observing a value of R_{obs}, given a particular lifetime ratio. The total likelihood function is now given by:

$$\mathcal{L} = \mathcal{L}_0 \times \frac{1}{\sqrt{2\pi}\sigma_{obs}} \exp\left[-\frac{(R(\tau_-/\tau_0) - R_{obs})^2}{2\sigma^2_{obs}}\right] \tag{8}$$

where σ_{obs} is the error on R_{obs}, and $\mathcal{L}_0$ is given in Eq. 5. The logarithm of $\mathcal{L}$ was maximised to determine the two free parameters τ_- and τ_0.

The values obtained are

$$\begin{aligned} \tau_0 &= 1.52^{+0.20}_{-0.18} \text{ ps} \\ \tau_- &= 1.47^{+0.22}_{-0.19} \text{ ps} \end{aligned}$$

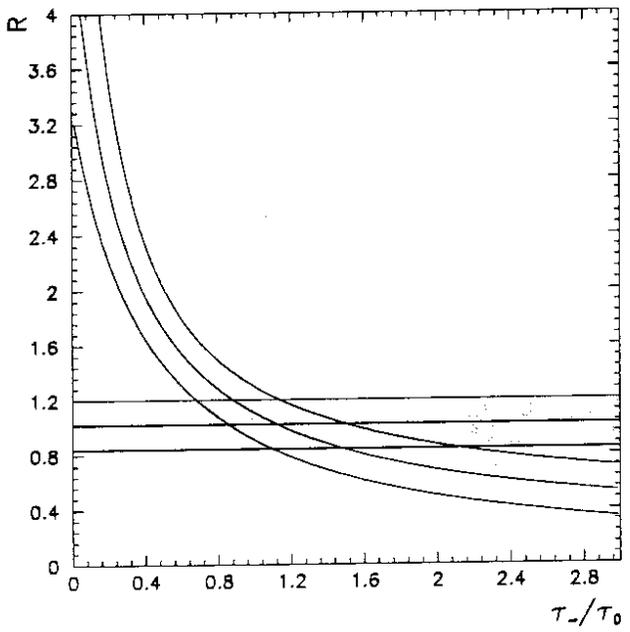

Figure 6: The expected ratio R (number of $D^{*+}\ell^-$ events divided by number of $D^0\ell^-$ events) as a function of the ratio of the lifetimes. The area bounded by the curves represents a 1σ variation of the $\bar{B}^0$ branching fractions. The horizontal line with the shaded area show the observed value and its error.

where the errors are statistical only. The correlation coefficient is 0.14. One may also consider the ratio of the lifetimes and their average to be the independent variables, in which case one obtains

$$\begin{aligned} \frac{\tau_-}{\tau_0} &= 0.96^{+0.19}_{-0.15} \\ \tau_{ave} &= 1.49^{+0.16}_{-0.14} \text{ ps} \end{aligned}$$

where, again, the errors are statistical only. The resulting curves of this simultaneous fit are superimposed on the proper time distributions in Fig. 5 (solid curves).

The fitted lifetime ratio results in following values for the sample compositions and the expected $D^{*+}\ell^- - D^0\ell^-$ ratio:

$$\begin{aligned} f_-^* &= 0.10^{+0.08}_{-0.10} \\ f_0^* &= 0.73^{+0.10}_{-0.08} \\ f_-^0 &= 0.63^{+0.06}_{-0.05} \\ f_0^0 &= 0.17^{+0.05}_{-0.06} \\ R &= 1.13 \pm 0.27 \end{aligned}$$

where the errors include the statistical uncertainty on τ_-/τ_0.

6 Systematic uncertainties

The following sources of systematic error have been considered:

- uncertainties arising from imprecise knowledge of the $\bar{B}^0$ semileptonic branching ratios;
- uncertainties in the background fractions and in the parametrizations of the background proper time distributions;
- uncertainties due to the smearing of the probability distribution used to correct for the missing neutrino (the κ distribution);
- uncertainties in the decay length resolution parametrization as obtained from the Monte Carlo simulation.

Imprecise knowledge of $\bar{B}^0$ semileptonic branching fractions leads to uncertainties in the calculated sample compositions and the expected event ratio R. The $\bar{B}^0$ branching fractions have been varied within their experimental errors, taking into account correlations, as described in detail in the Appendix.

Uncertainties in the background fractions and proper time distributions have been considered. Different background samples have been selected by varying the sideband regions and by using events with wrong-sign correlations, and alternative parametrizations of the proper time distributions have been studied.

The uncertainty in the κ distribution used to correct for the missing neutrino has been estimated by varying the parameters that influence its shape. The b quark fragmentation function, the number of events of the type $\bar{B}^0 \to D^{(*)}\pi\ell\nu$, and the event selection criteria have all been varied to determine the effect on κ and the resulting lifetimes.

The uncertainty due to the resolution function (Eq. 4) was estimated by allowing a variation of its parameters consistent with their statistical errors plus a systematic error due to uncertainty in the Monte Carlo model of the decay length resolution.

The various contributions to the systematic error for the full fit with the event ratio constraint are presented in Table 3. The total systematic error is dominated by the uncertainty on the $\bar{B}^0$ branching fractions. Furthermore, this uncertainty enters primarily through the calculation of R, the expected event ratio as a function of τ_-/τ_0. Systematic errors due to the different sources were combined in quadrature to obtain the total systematic error.

7 Final results and conclusions

A maximum likelihood fit to the proper time distributions of 77 $D^{*+}\ell^-$ and 77 $D^0\ell^-$ candidates and the relative observed rates of $D^{*+}\ell^-$ and $D^0\ell^-$ events has yielded the following $\bar{B}^0$ and B^- lifetimes and lifetime ratio:

$$\begin{aligned}
\tau_0 &= 1.52^{+0.20}_{-0.18}(\text{stat})^{+0.07}_{-0.13}(\text{syst}) \text{ ps} \\
\tau_- &= 1.47^{+0.22}_{-0.19}(\text{stat})^{+0.15}_{-0.14}(\text{syst}) \text{ ps} \\
\frac{\tau_-}{\tau_0} &= 0.96^{+0.19}_{-0.15}(\text{stat})^{+0.18}_{-0.12}(\text{syst})
\end{aligned}$$

Table 3: Sources of systematic error on the fitted lifetimes. The quantities B_ℓ, B_1, B_2 and z, which are used to calculate the $\bar{B}^0$ branching ratios, are defined in the Appendix.

Source of error		Contribution to systematic error		
		τ_0 (ps)	τ_- (ps)	τ_-/τ_0
B^0 branching ratios	B_ℓ	$^{+0.01}_{-0.02}$	$^{+0.03}_{-0.02}$	$^{+0.03}_{-0.02}$
	B_1	$^{+0.01}_{-0.02}$	± 0.02	$^{+0.03}_{-0.02}$
	B_2	$^{+0.02}_{-0.03}$	$^{+0.04}_{-0.03}$	$^{+0.04}_{-0.03}$
	z	$^{+0.06}_{-0.11}$	$^{+0.13}_{-0.12}$	$^{+0.17}_{-0.11}$
	Total	$^{+0.06}_{-0.12}$	$^{+0.14}_{-0.13}$	$^{+0.18}_{-0.12}$
Background treatment		± 0.02	± 0.03	± 0.03
κ distribution		± 0.03	± 0.03	± 0.01
Decay length resolution		± 0.01	± 0.01	± 0.01
Total		$^{+0.07}_{-0.13}$	$^{+0.15}_{-0.14}$	$^{+0.18}_{-0.12}$

Both τ_0 and τ_- are consistent with the average inclusive B hadron lifetime and the ratio of the lifetimes is consistent with unity.

The systematic error on the lifetimes is dominated by the uncertainty on the $\bar{B}^0$ semileptonic branching fractions, and in particular on the unmeasured ratio $\frac{D}{D+D^*}$ for decays of the type $\bar{B}^0 \to D^{(*)}\pi\ell\nu$. Furthermore, this uncertainty arises primarily in the calculation of the expected event ratio R (as opposed to the coefficients f_-^*, f_0^*, f_-^0 and f_0^0 of Eq. 5). This implies that for future, higher statistics, measurements of the B^- and $\bar{B}^0$ lifetimes, appropriate weighting of the event ratio information will be used to keep the systematic errors from this source at or below the level of the statistical errors.

8 Acknowledgements

It is a pleasure to thank our colleagues from the SL division for the operation of LEP. We are indebted to the engineers and technicians at CERN and our home institutes for their contributions to ALEPH's success. Those of us not from member states thank CERN for its hospitality.

Appendix - Determination of sample compositions

Table 4 shows the six $\bar{B}^0$ decay channels considered in the determination of the sample composition coefficients. Possible modes with two or more non-resonant

pions in the final state or with D^{**} decaying into $D^{(*)}$ plus two or more pions were assumed negligible. The branching ratios of the modes considered have been determined in the following way

1. B_1 and B_2 have been taken from measurements at CLEO and ARGUS [17, 18];

2. it was assumed that the inclusive semileptonic branching ratio of $\bar{B}^0$ mesons is given by the sum of the exclusive channels considered,

$$B_\ell \equiv B(\bar{B}^0 \to \ell^- X) = \sum_{i=1}^{6} B_i.$$

   This quantity has also been measured at CLEO and ARGUS [5, 18, 19];

3. it was assumed that, in decays of the type $\bar{B} \to D^{(*)}\pi\ell\nu$ the $D^{(*)}\pi$ states are produced with a fixed value of isospin, $I = 1/2$ (as is the case if the decay proceeds via D^{**}). Then isospin conservation implies

$$n \equiv \frac{B_4}{B_3} = \frac{B_6}{B_5} = 2.$$

4. the quantity

$$z \equiv \frac{B_5}{B_3 + B_5}$$

   has not been measured. A value of $z = 0.5 \pm 0.5$ was assumed.

The conditions 2–4 allow the calculation of B_3–B_6. The uncertainties on these branching ratios are large and highly correlated and thus not very meaningful. The quantities B_ℓ, B_1, B_2 and z are the independent quantities used to calculate the $\bar{B}^0$ semileptonic branching fractions. They have been varied independently for the evaluation of the systematic error on the fitted lifetimes. As explained in the main part of this Letter, the B^- branching ratios were obtained using Eq. 6.

The contributions to the $D^{*+}\ell^-$ and $D^0\ell^-$ samples were calculated using these branching ratios, the branching ratio for $D^{*+} \to D^0\pi^+$ ($B_* = 0.68 \pm 0.03$ [20]), and the relative efficiency for detecting channels B_3–B_6 ($\epsilon^{**} = 0.70 \pm 0.03$, determined using a Monte Carlo simulation). The probability that a $D^{*+}\ell^-$ event is mistakenly reconstructed as a $D^0\ell^-$ event ($\epsilon_{\delta m} = 0.15 \pm 0.02$) was also taken into account. Table 5 shows the $\bar{B}^0$ and B^- contributions to the $D^{*+}\ell^-$ and $D^0\ell^-$ samples.

Table 4: $\bar{B}^0$ semileptonic branching ratios. The corresponding B^- decay channels are also listed. The uncertainties on B_3–B_6 are large and highly correlated and therefore are not shown.

$\bar{B}^0$ BR (%)		Corresponding B^- Decay
$B_1 = B(\bar{B}^0 \to D^{*+}\ell^-\nu)$	$= 4.74 \pm 0.38$	$B_1^- = B(B^- \to D^{*0}\ell^-\nu)$
$B_2 = B(\bar{B}^0 \to D^{+}\ell^-\nu)$	$= 1.84 \pm 0.51$	$B_2^- = B(B^- \to D^{0}\ell^-\nu)$
$B_3 = B(\bar{B}^0 \to D^{*+}\pi^0\ell^-\nu)$	$= 0.49$	$B_3^- = B(B^- \to D^{*0}\pi^0\ell^-\nu)$
$B_4 = B(\bar{B}^0 \to D^{*0}\pi^+\ell^-\nu)$	$= 0.97$	$B_4^- = B(B^- \to D^{*+}\pi^-\ell^-\nu)$
$B_5 = B(\bar{B}^0 \to D^{+}\pi^0\ell^-\nu)$	$= 0.49$	$B_5^- = B(B^- \to D^{0}\pi^0\ell^-\nu)$
$B_6 = B(\bar{B}^0 \to D^{0}\pi^+\ell^-\nu)$	$= 0.97$	$B_6^- = B(B^- \to D^{+}\pi^-\ell^-\nu)$
$B_\ell = B(\bar{B}^0 \to \ell X)$	$= 9.50 \pm 1.40$	

Table 5: Contributions of $\bar{B}^0$ and B^- decays to the $D^{*+}\ell^-$ and $D^0\ell^-$ event samples.

	$D^{*+}\ell^-$	$D^0\ell^-$
$\bar{B}^0$	$B_* B_1 + \epsilon^{**} B_* B_3$	$\epsilon_{\delta m}(B_* B_1 + \epsilon^{**} B_* B_3) + \epsilon^{**}(B_4 + B_6)$
B^-	$\frac{\tau_-}{\tau_0}[\epsilon^{**} B_* B_4]$	$\frac{\tau_-}{\tau_0}[B_1 + B_2 + \epsilon^{**}(B_3 + B_5) + \epsilon^{**}\epsilon_{\delta m} B_* B_4)]$

References

[1] D. Decamp, *et al.* (ALEPH Collab.), Phys. Lett. B **257** (1991) 492.
B. Adeva, *et al.* (L3 Collab.), Phys. Lett. B **270** (1991) 111.
P. Abreu, *et al.* (DELPHI Collab.), Z. Phys. C. **53** (1992) 567.
P. Acton, *et al.* (OPAL Collab.), Phys. Lett. B **274** (1992) 513.

[2] B. Buskulic, *et al.* (ALEPH Collab.), Phys. Lett. B **295** (1992) 174.

[3] S. Wagner, *et al.* (MarkII Collab.), Phys. Rev. Lett. **64** (1990) 1095.
P. Abreu, *et al.* (DELPHI Collab.), CERN-PPE/92-174 (1992), to be published in Z. Phys. C.
B. Buskulic, *et al.* (ALEPH Collab.), Phys. Lett. B **297** (1992) 449.

[4] H. Albrecht, *et al.* (ARGUS Collab.), Phys. Lett. B **275** (1992) 195.
R. Fulton, *et al.* (CLEO Collab.), Phys. Rev. **D43** (1991) 236.

[5] D. S. Akerib, *et al.*, (CLEO Collab.), "A Measurement of the Charged and Neutral B Meson Lifetime Ratio," contributed paper to the XXVI International Conference on High Energy Physics, August 1992, Dallas, USA.

[6] M. B. Voloshin and M. A. Shifman, Sov. Phys. JETP **64** (1986) 698
I. Bigi and N. Uraltsev, Phys. Lett. B **280** (1992) 271.

[7] D. Decamp *et al.* (ALEPH Collaboration), Nucl. Instrum. Methods A **294** (1990) 121.

[8] G. Batignani *et al.*, "Recent Results and Running Experience of the New ALEPH Vertex Detector", Conference Record of the 1991 IEEE Nuclear Science Symposium, November 2-9, 1991, Santa Fe, New Mexico, USA.

[9] D. Decamp, *et al.* (ALEPH Collab.), Z. Phys. C. **53** (1992) 1.

[10] D. Decamp, *et al.* (ALEPH Collab.), Phys. Lett. B **263** (1991) 325.

[11] D. Decamp, *et al.* (ALEPH Collab.), Phys. Lett. B **279** (1992) 411.

[12] D. Decamp, *et al.* (ALEPH Collab.), Phys. Lett. B **266** (1991) 218.

[13] B. Buskulic, *et al.* (ALEPH Collab.), Phys. Lett. B **294** (1992) 145.

[14] D. Bortoletto, *et al.* (CLEO Collab.), Phys. Rev. Lett. **64** (1990) 2117.
H. Albrecht, *et al.* (ARGUS Collab.), Z. Phys. C. **54** (1992) 1.

[15] S. Godfrey and N. Isgur, Phys. Rev. D **32** (1985) 189.

[16] Particle Data Group, Phys. Rev. D **45**, Part 2 (1992).

[17] D. Bortoletto, *et al.* (CLEO Collab.), Phys. Rev. Lett. **63** (1989) 1667.
R. Fulton, *et al.* (CLEO Collab.), Phys. Rev. D **43** (1991) 651.
H. Albrecht, *et al.* (ARGUS Collab.), preprint DESY 92-039, February 1992.

[18] Yu. Zaitsev, "Selected ARGUS results on B meson decays," to be published in the proceedings of the XXVI International Conference on High Energy Physics, August 1992, Dallas, USA.

[19] S. Henderson, *et al.* (CLEO Collab.), Phys. Rev. D **45** (1992) 2212.

[20] F. Butler, *et al.* (CLEO Collab.), Phys. Rev. Lett. **69** (1992) 2041.